PHYSICAL REVIEW A **89**, 033419 (2014)

Three-level superadiabatic quantum driving

Luigi Giannelli[1] and Ennio Arimondo[1,2]
[1]*Dipartimento di Fisica, Università di Pisa, Largo Pontecorvo 3, 56127 Pisa, Italy*
[2]*INO-CNR, Università di Pisa, Largo Pontecorvo 3, 56127 Pisa, Italy*
(Received 1 February 2014; published 17 March 2014)

The superadiabatic quantum driving, producing a perfect adiabatic transfer on a given Hamiltonian by introducing an additional Hamiltonian, is theoretically analyzed for transfers within a three-level system. Our starting point is the stimulated Raman adiabatic passage, realized through different schemes of laser pulses. We determine the superadiabatic correction for each scheme. The fidelity, robustness, and transfer time of all the superadiabatic transfer schemes are discussed. We derive that all superadiabatic corrections are based on a π- (or near-π)-area pulse coupling between the initial and final states. The benefits in the protocol robustness overcome the difficulties associated to the actual implementation of the three-level superadiabatic transfer.

DOI: 10.1103/PhysRevA.89.033419 PACS number(s): 32.80.Qk, 42.50.Hz

I. INTRODUCTION

The ability to accurately control a quantum system is a fundamental requirement in many areas of modern science ranging from quantum information processing and coherent manipulation of quantum systems to high-precision measurements. Very often the quantum control aims at reaching a given target state, as in the preparation of a given atomic or molecular state, or the cooling of atomic ensembles and nanomechanical oscillators. The optimum strategy designed for a given task complies with the requirements of a nearly perfect fidelity of the final state, of an operation speed close to the quantum speed natural lower bound limit rooted in the Heisenberg uncertainty principle, and finally of robustness against imperfections in the quantum control protocol.

Superadiabatic [1,2] or transitionless [3–5] protocols and shortcuts to adiabaticity [6] have recently received much attention for the realization of the above targets. In the superadiabatic or transitionless protocols the controlled system follows perfectly the instantaneous adiabatic ground state of a given Hamiltonian following the application of an *ad hoc* additional Hamiltonian. The shortcuts to adiabaticity are based on the preparation of the controlled system into eigenstates of the Hamiltonian invariants that characterize all the transformations of the given Hamitonian. The superadiabatic protocols were recently tested on two-level systems: an energy-level anticrossing for a Bose-Einstein condensate loaded into an optical lattice [7–9] and the magnetic resonance of a one-half spin [10]. Those experiments demonstrated that superadiabatic protocols realize quantum fidelity equal to 1, speed close to the quantum limit, and robustness against parameter variations, making them useful for practical applications. Protocols based on the Hamiltonian invariants have not been tested experimentally so far.

The theoretical treatment for the superadiabatic transformations [2] provides a quite general approach valid for any multilevel system. The present work applies the superadiabatic transformation to the population transfer in a three-level system. The process of stimulated Raman adiabatic passage (STIRAP) allows us to produce an adiabatic passage with the use of two constant frequency suitably delayed laser pulses [11,12]. The high fidelity requirement is achieved using large pulse areas, i.e., large average Rabi frequencies and long interaction times. For several applications this requirement is a critical disadvantage. Superadiabatic STIRAP (sa-STIRAP) protocols allow a perfect three-level transfer without the need of intense pulses or long transfer times.

We determine several sa-STIRAP protocols, generalizing the previous investigations of Demirplak and Rice [3,4] and of Chen *et al.* [13]. The fidelity of the three-level STIRAP and sa-STIRAP protocols, their robustness against variations of the different parameters, and their transfer speeds are calculated. Our analysis demonstrates that any sa-STIRAP configuration requires the application of an additional pulse having a π (or near-π) area producing a direct transfer between the initial and final states, as stated in Refs. [13–15] for Gaussian laser pulses. We demonstrate that a very high fidelity can be reached even releasing that requirement. The analysis of fidelity and robustness is applied also to another scheme of three-level transfer based on the Hamiltonian invariants recently developed by Cheng and Muga [16]. Our attention is focused on quantum computation applications of three-level systems where fidelities close to 1 within one part in a thousand is required.

Section II introduces the three-level system, the standard STIRAP laser scheme, and also the protocol developed in Ref. [16] based on the Hamitonian invariants. Section III derives the sa-STIRAP Hamiltonian. The realization of the Hamiltonian matrix element connecting the initial and final states required to implement the sa-STIRAP is also presented there. Section IV reports numerical analyses of the important features, fidelity, losses, robustness, and transfer time for all the previous introduced protocols. Section V concludes our work.

II. HAMILTONIAN AND STIRAP

A. Three-level Hamiltonian

The basic STIRAP process involves three quantum states, linked by two time-dependent interactions to be referred to as pump, at frequency ω_p between state $|1\rangle$ of energy E_1 and the excited state $|2\rangle$ having energy E_2, and Stokes interaction, at frequency ω_s, between the intermediate state $|2\rangle$ and the final target state $|3\rangle$ having energy E_3. Two different energy level configurations will be examined, the ladder one with $E_3 > E_2$ and the Λ one with $E_3 < E_2$. The Hamiltonian within the rotating wave approximation [11,17]) reads as in the

following:

$$H^0(t) = \frac{\hbar}{2}\begin{pmatrix} 0 & \Omega_p(t) & 0 \\ \Omega_p(t) & 2\Delta_p & \Omega_s(t) \\ 0 & \Omega_s(t) & 2\Delta_3 \end{pmatrix}, \tag{1}$$

with Ω_p and Ω_s the pump and Stokes Rabi frequencies. The detunings from resonance are defined by $\Delta_p = \omega_p - (E_2 - E_1)/\hbar$, $\Delta_s = \omega_s - (|E_3 - E_2|)/\hbar$, and $\Delta_3 = \Delta_p + \Delta_s$ for the ladder configuration, and $\Delta_3 = \Delta_p - \Delta_s$ for the Λ configuration.

Since the phases of the pump and Stokes fields can be included into the $|1\rangle$ and $|3\rangle$ definitions without loss of generality, the Rabi frequency will be chosen real, except in the Appendix. We define an effective Rabi frequency Ω_0, denoted as adiabatic energy in [18],

$$\Omega_0(t) = \sqrt{\Omega_p(t)^2 + \Omega_s(t)^2}. \tag{2}$$

Population losses with a Γ_2 rate from the $|2\rangle$ intermediate level will be introduced into our model. We will analyze the case of an open system with the $|2\rangle$ state decaying to a state external to the three-level system. That represents an example of the sa-STIRAP strength to eliminate all kinds of losses.

For the transfer process of our interest it is essential to apply the $\Delta_3 = 0$ two-photon resonance condition, and this case will be here examined. The three-level analysis can be written in a simpler form by defining

$$\tan\theta(t) = \frac{\Omega_p(t)}{\Omega_s(t)}, \quad \tan\phi(t) = \frac{\Omega_0(t)}{\Delta_p + \sqrt{\Delta_p^2 + \Omega_0(t)^2}}, \tag{3}$$

with

$$\dot\theta(t) = \frac{\dot\Omega_p(t)\Omega_s(t) - \Omega_p(t)\dot\Omega_s(t)}{\Omega_0(t)^2}. \tag{4}$$

The Hamiltonian eigenvalues are written as

$$\begin{aligned} \lambda_0(t) &= 0, \\ \lambda_-(t) &= -\frac{\hbar}{2}\Omega_0(t)\tan\phi(t), \\ \lambda_+(t) &= \frac{\hbar}{2}\Omega_0(t)\cot\phi(t) \end{aligned} \tag{5}$$

and the instantaneous eigenvectors are [11,19]

$$\begin{aligned} |a_0(t)\rangle &= \begin{pmatrix} \cos\theta(t) \\ 0 \\ -\sin\theta(t) \end{pmatrix}, \\ |a_-(t)\rangle &= \begin{pmatrix} \sin\theta(t)\cos\phi(t) \\ -\sin\phi(t) \\ \cos\theta(t)\cos\phi(t) \end{pmatrix}, \\ |a_+(t)\rangle &= \begin{pmatrix} \sin\theta(t)\sin\phi(t) \\ \cos\phi(t) \\ \cos\theta(t)\sin\phi(t) \end{pmatrix}. \end{aligned} \tag{6}$$

As the three-level key feature, the $|a_0(t)\rangle$ eigenstate is a dark state with zero projection on state $|2\rangle$.

B. STIRAP

The STIRAP protocol allows us to produce an efficient transfer from $|1\rangle$ as initial state to $|3\rangle$ as final state [11,12] following the evolution of the $|a_0\rangle$ dark state. Within the (t_i,t_f) time interval the pump and Stokes lasers are applied as pulses satisfying the well-known counterintuitive sequence with Ω_s first and Ω_p later, as in Fig. 1.

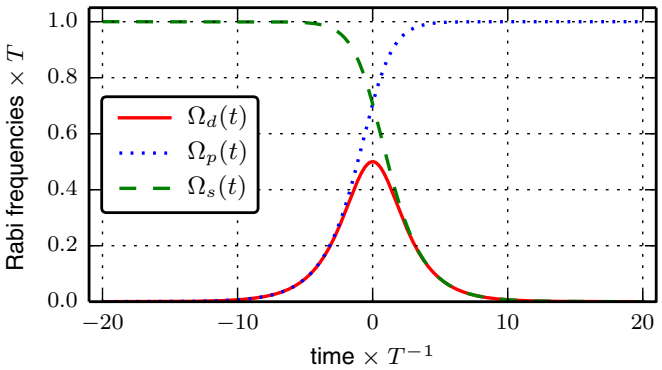

FIG. 1. (Color online) Time dependencies of the Ω_p and Ω_s STIRAP exponential pulses (line 2 of Table I) and of the Ω_d sa-STIRAP correction. $\Omega_T = 1$ in the dimensionless units of Eq. (26).

We consider the STIRAP pulses listed in the top part of Table I, most of them written as

$$\Omega_p(t) = \Omega_{\text{peak}} f\left(\frac{t-\tau}{T}\right), \quad \Omega_s(t) = \alpha\Omega_{\text{peak}} f\left(\frac{t+\tau}{T}\right), \tag{7}$$

where $f(t)$ is a pulse envelope having unit maximum value, Ω_{peak} is the peak Rabi frequency, 2τ is the delay between pulses, and T is the pulse width. α is a scaling parameter, smaller than 1, introduced for two protocols of Table I where the Ω_s maximum is smaller than the Ω_p one. The counterintuitive sequence condition imposes $\tau > 0$. Table I includes the sin-cos protocol introduced in Ref. [18] and rederived in Ref. [16] through the Hamiltonian invariant approach. Few protocols, for instance the exponential of line 2 and the sin-cos of line 4, have finite Rabi frequencies applied at initial or final times. For these protocols, outside the STIRAP time interval Ω_s and Ω_p should be adiabatically switched on/off, respectively.

The Rabi frequencies of the above protocols satisfy the following relations:

$$\begin{aligned} \lim_{t\to t_i}\frac{\Omega_p(t)}{\Omega_s(t)} &= \lim_{t\to t_i}\tan\theta(t) = \epsilon_1, \\ \lim_{t\to t_f}\frac{\Omega_s(t)}{\Omega_p(t)} &= \lim_{t\to t_f}\operatorname{cotan}\theta(t) = \epsilon_2, \end{aligned} \tag{8}$$

with ϵ_1,ϵ_2 small quantities, equal to zero for protocols on top of Table I and different from zero for those on the bottom. The Rabi frequencies' temporal dependence implies

$$\lim_{t\to t_i}\theta(t) = \epsilon_1, \quad \lim_{t\to t_f}\theta(t) = \pm\frac{\pi}{2} - \epsilon_2. \tag{9}$$

Thus within the (t_i,t_f) time interval, $\theta(t)$ varies from ϵ_1 to $\pm\frac{\pi}{2} - \epsilon_2$. For $\epsilon_1 = \epsilon_2 = 0$ the $|a_0(t)\rangle$ dark state varies from $|1\rangle$ to $|3\rangle$, while for $\epsilon_1,\epsilon_2 \neq 0$ the $|a_0(t)\rangle$ wave function contains at

TABLE I. Temporal dependencies of $\Omega_p/\Omega_{\rm peak}$ and $\Omega_s/\Omega_{\rm peak}$ in STIRAP schemes, and of Ω in sa-STIRAP schemes. In last column the ϵ_1,ϵ_2 deviations of Ω_d from a perfect π area pulse. For $\sin^4$ pulses Ω_p and Ω_s are different from 0 in the $(\tau < t < \tau + T)$ and $(-\tau < t < T - \tau)$ intervals, respectively; for sin-cos pulses both are different from 0 for $(0 < t < T)$.

$\Omega_p(t)/\Omega_{\rm peak}$	$\Omega_s(t)/\Omega_{\rm peak}$	$\Omega_d(t)$	(ϵ_1,ϵ_2)	Ref.
$e^{-[(t-\tau)/T]^2}$	$e^{-[(t+\tau)/T]^2}$	$4\tau[T^2\cosh(\frac{4\tau t}{T^2})]^{-1}$	(0,0)	[18]
$(1+e^{-t/T})^{-1/2}$	$(1+e^{+t/T})^{-1/2}$	$[2T\cosh(\frac{t}{2T})]^{-1}$	(0,0)	[18]
$\sin^4\frac{\pi(t-\tau)}{T}$	$\sin^4\frac{\pi(t+\tau)}{T}$	$\frac{\pi}{T}\sin\frac{2\tau\pi}{T}(\cos\frac{2\pi\tau}{T}-\cos\frac{2\pi t}{T})^3\{\sin^8[\frac{\pi}{T}(t-\tau)]+\sin^8[\frac{\pi}{T}(t+\tau)]\}^{-1}$	(0,0)	[19]
$\sin[\frac{1}{2}\arctan\frac{t}{T}+\frac{\pi}{4}]$	$\cos[\frac{1}{2}\arctan\frac{t}{T}+\frac{\pi}{4}]$	$T[t^2+T^2]^{-1}$	(0,0)	[20,21]
$\sin(\frac{\pi t}{2T})$	$\cos(\frac{\pi t}{2T})$	πT^{-1}	(0,0)	[16,18]
$\frac{1}{T}\operatorname{sech}\frac{t}{T}$	$\frac{\alpha}{T}\sqrt{(1-\tanh\frac{t}{T})}$	$4\alpha e^{t/T}[T\sqrt{2}(\alpha^2+e^{2t/T}(2+\alpha^2))\sqrt{1+e^{2t/T}}]^{-1}$	$(0,\sqrt{2}\alpha)$	[22]
$\frac{1}{T}\sqrt{(1-\tanh\frac{t}{T})}\operatorname{sech}\frac{t}{T}$	$\frac{\alpha}{T}(1-\tanh\frac{t}{T})$	$4\alpha e^{t/T}[T\sqrt{2}(\alpha^2+e^{2t/T}(2+\alpha^2))\sqrt{1+e^{2t/T}}]^{-1}$	$(0,\sqrt{2}\alpha)$	[22]
$\operatorname{sech}\frac{t-\tau}{T}$	$\operatorname{sech}\frac{t+\tau}{T}$	$2\sinh\frac{2\tau}{T}T^{-1}[1+\cosh\frac{2t}{T}\cosh\frac{2\tau}{T}]^{-1}$	$(e^{-2\tau/T}e^{-2\tau/T})$	[18]

initial and final times both $|1\rangle$ and $|3\rangle$ contributions, therefore a small coherence between those states. We have not included in our analysis other protocols based on the presence of a large initial three-level coherence as in [16,21], and of higher-order trapping states as in Ref. [21].

The local adiabaticity condition for a transfer via the $|a_0\rangle$ eigenstate is [11,23]

$$|\dot\theta(t)| \ll \tfrac{1}{2}\left|\Delta_p \pm \sqrt{\Delta_p^2+\Omega_0(t)^2}\right|. \tag{10}$$

By assuming $\Delta_p(t) \ll \Omega_p(t),\Omega_s(t)$, a global adiabaticity condition is derived by time averaging Eq. (10) over the τ characteristic time of the $\Omega_p(t)$ and $\Omega_p(t)$ overlap. For the pulses of Eq. (7) using Eq. (9) the global condition becomes

$$\Omega_{\rm peak}\tau \gg 1. \tag{11}$$

III. SA-STIRAP PROTOCOLS

A. Hamiltonian

Following Refs. [1–5] the superadiabatic approach requires the application of a total Hamiltonian

$$H(t) = H^0(t) + H^1(t), \tag{12}$$

with the superadiabatic correction

$$H^1(t) = i\hbar\sum_n [|\partial_t n\rangle\langle n| - \langle n|\partial_t n\rangle|n\rangle\langle n|] \tag{13}$$

determined from the instantaneous eigenvalues $|n(t)\rangle = (|a_0\rangle,|a_-\rangle,|a_+\rangle)$.

By applying $H(t)$ the system evolution will follow exactly the instantaneous eigenstate of the H^0 STIRAP Hamiltonian. If the system initial state is in the dark one, the system will remain in that dark state at all times. The adiabatic following of the STIRAP $H^0(t)$ eigenstates takes place for any choice of the protocol parameters, even with very small values of the applied pump and Stoke fields, and in arbitrary short time.

Using Eqs. (6) the Hermitian H^1 Hamiltonian becomes

$$H^1(t) = \hbar\begin{pmatrix} 0 & i\dot\phi(t)\sin\theta(t) & i\dot\theta(t) \\ -i\dot\phi(t)\sin\theta(t) & 0 & -i\dot\phi(t)\cos\theta(t) \\ -i\dot\theta(t) & i\dot\phi(t)\cos\theta(t) & 0 \end{pmatrix}. \tag{14}$$

with the matrix elements given by

$$\dot\phi(t)\sin\theta(t) = \frac{\Omega_p(\dot\Delta_p\Omega_0 - \Delta_p\dot\Omega_0)}{2\Omega_0(\Delta_p^2+\Omega_0^2)}, \tag{15}$$

$$\dot\phi(t)\cos\theta(t) = \frac{\Omega_s(\dot\Delta_p\Omega_0 - \Delta_p\dot\Omega_0)}{2\Omega_0(\Delta_p^2+\Omega_0^2)}, \tag{16}$$

and $\dot\theta(t)$ given by Eq. (4). For $\dot\Delta_p(t) = 0$ the above equations reduce to those reported in Ref. [13]. For real phases of the pump and Stokes Rabi frequencies, all the H^1 elements are purely imaginary; for not-real phases see the Appendix.

The $H^1_{12}(t)$ and $H^1_{23}(t)$ matrix elements represent a correction to the pump and Stokes pulses. They impose a phase relation between their Rabi frequencies and modify their temporal dependence. These matrix elements vanish in the trivial case $\Omega_p(t) = \Omega_s(t) = \Omega_0(t) = 0$, $\Delta_p(t) \neq 0$, or in the more interesting case of

$$\Delta_p(t) = C\Omega_0(t). \tag{17}$$

Here C is any constant, also zero, leading to the convenient choice of $\Delta_p(t)$ a constant equal to zero for annulling those corrections.

The most interesting $H^1_{13}(t)$ matrix element couples directly the initial and final states. It will be written as

$$H^1_{13}(t) = \hbar\frac{i\Omega_d(t)}{2}, \tag{18}$$

having defined the *detuning pulse* as

$$\Omega_d(t) \equiv 2\dot\theta(t). \tag{19}$$

Such definition was introduced in Ref. [14] and analyzed in Ref. [21] because in the $|a_n(t)\rangle$ basis, $\Omega_d(t)$ represents

a detuning energy of the $|a_0(t)\rangle$ dark state. In the $|1,2,3\rangle$ basis $i\Omega_d(t)$ represents a Rabi frequency connecting states $|1\rangle$ and $|3\rangle$. Because the H^1 Hamiltonian is written within the rotating-wave approximation, the $i\Omega_d$ Rabi coupling is created by a field oscillating at frequency $\omega_p - \omega_s$ in the Λ configuration, and frequency $\omega_p + \omega_s$ in the ladder one. The $\Omega_d(t)$ functions associated to the different STIRAP pulses are reported in the last column of Table I, and that for the exponential pulses is plotted in Fig. 1.

If a proper time dependence of $\Omega_p(t)$ and $\Omega_s(t)$ could be found such that the detuning pulse, i.e., $H^1_{13}(t)$, is identically zero, a superadiabatic evolution of the system could be produced only by changing the shape of the pump and Stokes fields. But this is not the case because $\Omega_d(t) = 0$ only if

$$\Omega_p(t) \propto \Omega_s(t). \tag{20}$$

For this noncounterintuitive configuration the $|a_0(t)\rangle$ dark state does not link anymore the $|1\rangle$ and $|3\rangle$ states. The Appendix deriving $\Omega_d(t)$ in the presence of a time dependence of the pump and Stokes field phases demonstrates that also in that case the $H^1_{13}(t) = 0$ requirement cannot be satisfied. While the key role of $\dot{\theta}$ in controlling the nonadiabaticity of STIRAP was pointed out by several authors, see [18,21], we derive that the $\dot{\theta}$ Rabi frequency coupling between initial and final states is strictly required in the sa-STIRAP realization.

The time dependence of $\Omega_d(t)$, i.e., $\dot{\theta}(t)$, is determined by Eq. (4). Using Eq. (9) for our STIRAP pulses, that time dependence leads to

$$\int_{t_i}^{t_f} \Omega_d(t)dt = \int_{t_i}^{t_f} 2\dot{\theta}(t)dt = \pm\pi - 2(\epsilon_1 + \epsilon_2). \tag{21}$$

Therefore the $\Omega_d(t)$ dependence corresponds to a nearly π-area pulse, a perfect one for several pulses, for instance the Gaussian one, as shown by the ϵ_1,ϵ_2 values in the last column of Table I. Notice that a resonant π-area pulse connecting the states $|1\rangle$ and $|3\rangle$ produces a complete population transfer by itself. Thus we obtain a deceiving result: the superadiabatic STIRAP realization implies the application of an additional electromagnetic field that in the π-area pulse configuration produces by itself the required transfer. As investigated in the following, the combination of STIRAP and near π-area detuning pulses becomes useful when examining the robustness of the different transfer schemes. The π-area pulse requirement was derived in [14,21] while searching for an improvement of the STIRAP efficiency by adding a low-frequency field. We have demonstrated that the near π-area pulse condition derives from the superadiabatic construction and leads to the complete cancellation of the nonadiabatic losses.

B. Detuning pulse realization

1. Magnetic-dipole in Λ scheme

Owing to the parity selection rules, in the Λ systems of Figs. 2(a) and 2(b) the $i\Omega_d$ coupling between the $|1\rangle$ and $|3\rangle$ states may be originated by a magnetic dipole interaction between the **J** atomic or molecular angular momentum and an external magnetic field **B**,

$$H_B = \mu_B g_J \mathbf{J}\cdot\mathbf{B}, \tag{22}$$

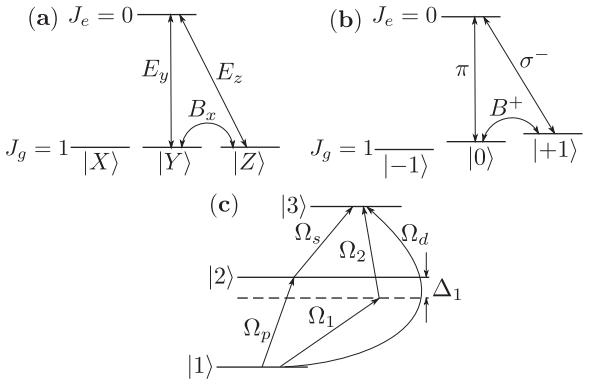

FIG. 2. In (a) and (b) sa-STIRAP realization in a Λ system between the $J_g = 1$ Zeeman sublevels and an excited $J_e = 0$ state. (a) Laser configuration defined within a Cartesian $|i\rangle, (i = X,Y,Z)$ basis set with linearly polarized lasers and static magnetic field B_x. (b) Laser configuration defined in the basis of the J_z eigenstates with π/σ^- lasers and a σ^+ circularly polarized magnetic radio frequency field. (c) sa-STIRAP in a ladder system with the the detuning pulse produced by an additional two-photon transition.

μ_B being the Bohr magneton and g_J the Landé factor. The detuning pulse is

$$\frac{i\Omega_d(t)}{2} = \mu_B g_J \frac{\langle 1|\mathbf{J}\cdot\mathbf{B}(t)|3\rangle}{\hbar}. \tag{23}$$

As proposed in Ref. [14] that magnetic coupling may be realized for a $J_g = 1$ ground state and an excited $J_e = 0$ state. A Λ system with two ground Zeeman states and the excited state is selected by properly choosing the laser polarizations. In the $|X\rangle$, $|Y\rangle$, and $|Z\rangle$ Cartesian basis of the $J_g = 1$ state and for pump and Stokes laser fields linearly polarized along the y and z axis, the scheme works out with $|1\rangle = |Y\rangle$ and $|3\rangle = |Z\rangle$, as in Fig. 2(a). A B_x magnetic field along the x axis produces the imaginary detuning pulse,

$$\langle Y|H_{13}|Z\rangle = i\hbar\frac{\Omega_d(t)}{2} = -i\mu_B g_J B_x. \tag{24}$$

Another simple realization based on the spherical basis of the $J_g = 1$ state is shown in Fig. 2(b) in the presence of a magnetic splitting between the $|J_g,m_J = 0\rangle$ and $|J_g,m_J = 1\rangle$ Zeeman sublevels. In this case the pump and Stokes fields have π and σ^- polarizations and the detuning pulse is based on a σ^+ circularly polarized resonant radio frequency magnetic field **B** in the x-y plane. This field phase should be $\pi/2$ shifted in respect to that of $\omega_p - \omega_s$. The generalization of these schemes to different atomic configurations is not obvious.

2. Two-photon transition in ladder

In a ladder level scheme the direct interaction between states $|1\rangle$ and $|3\rangle$ may take place via a two-photon transition, as in Fig. 2(c). Two new lasers with Rabi frequencies $\Omega_1(t)$ and $\Omega_2(t)e^{i(\pi/2)}$ are added to the system in order to satisfy the two-photon resonance. The one-photon resonance is detuned by Δ_1 from the $|2\rangle$ intermediate state. We impose the sa-STIRAP $H^1_{13}(t)$ matrix element of Eq. (18) equal to the two-photon Rabi

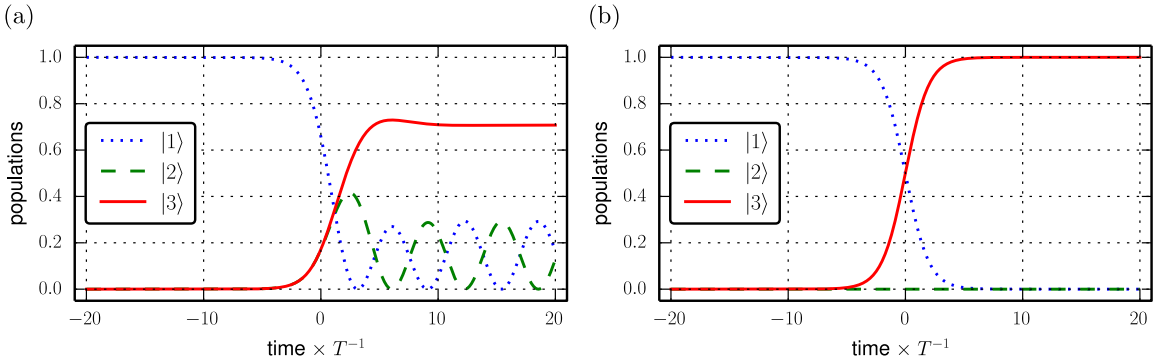

FIG. 3. (Color online) Time dependence of the $|1,2,3\rangle$ populations for the STIRAP and sa-STIRAP exponential protocols in (a) and (b), respectively, for $\Omega_T = 1$. $\Gamma_2 = 0$ in all cases.

frequency [24] and obtain

$$i\frac{\Omega_d(t)}{2} = -\frac{\Omega_1(t)\Omega_2(t)e^{-i(\pi/2)}}{2\cdot 2\Delta_1} = i\frac{\Omega_1(t)\Omega_2(t)}{4\Delta_1}. \tag{25}$$

At fixed Δ_1 a simple choice is to $\Omega_1(t) = \Omega_2(t) = \sqrt{2\Delta_1\Omega_d(t)}$. For an experimental realization of this scheme two sidebands of the pump and Stokes frequencies at radio frequencies ω_{rf} and $-\omega_{rf}$, respectively, could be created. In addition by imposing a 90° phase shift of the radio frequency fields the imaginary sign of the detuning field can be produced.

IV. NUMERICAL ANALYSES

This section derives fidelity, robustness, population loss from the intermediate state, robustness, and speed-limit for the STIRAP or sa-STIRAP protocols having $\epsilon_1 = \epsilon_2 = 0$. Four parameters describe the laser and atom evolutions: (i) the Ω_{peak}peak Rabi frequency, (ii) the T laser pulses duration, (iii) the 2τ delay between pulses measuring their overlap, and (iv) the Γ_2 decay rate of the $|2\rangle$ state. The system evolution is characterized by a time-scale invariance. Then for all values of the previous parameters, except for a time-scale factor, the system evolution is fully defined by three quantities:

$$\Omega_T = \Omega_{\text{peak}}T, \quad \tau_T = \frac{\tau}{T}, \quad \Gamma_T = \Gamma_2 T. \tag{26}$$

That is easily verified for the Gaussian pulses, and it was numerically verified also for other pulses. In the following we will use $T = 1$ μs as reference time scale, and the presented plots should be properly scaled for analyzing other pulse durations.

A. Fidelity

The following fidelity characterizes completely the $|\Psi(t)\rangle$ wave-function transfer to the $|3\rangle$ state:

$$F = |\langle 3|\Psi(t_{\text{fin}})\rangle|^2. \tag{27}$$

For the $\Gamma_2 = 0$ case $F > 0.95$ values are achieved applying a STIRAP protocol with area parameter $A = \Omega_{\text{peak}}\tau$ around 10–20. Therefore the sa-STIRAP protocol is useful mainly at low values of A, where the STIRAP fidelity greatly depends on the $f(t)$ temporal dependence. For the exponential pulses of Fig. 1 with $\tau_T = \Omega_T = 1$ STIRAP produces a maximum final fidelity around 0.7, as in Fig. 3(a). Instead the sa-STIRAP final fidelity is 1 for all the τ, Ω_{peak} values, as in Fig. 3(b).

For a quantum computation target, where $F > 0.999$ fidelities are required, the STIRAP protocol is not good enough, as it appears in Fig. 4 for the Gaussian protocol. Its fidelity is characterized by an oscillating dependence on the Ω_T parameter, with the required very high fidelities reached only in narrow parameter regions. A similar oscillating dependence occurs also for exponential STIRAP pulses, with reduced oscillation amplitude. For the sin-cos transfer protocol of Table I Chen *et al.* [16] presented the following oscillating dependence of F on the Ω_{peak} value:

$$\sqrt{F} = 1 - \sin^2\epsilon\left[1 - \cos\left(\frac{\pi}{1\sin\epsilon}\right)\right], \tag{28}$$

with $\epsilon = \text{arccot}(\Omega_T/\pi)$. This dependence is also shown in Fig. 4. In all cases the $F = 1$ maxima appear when the Rabi oscillations between the system levels are in phase with the interaction time. The successive maxima are obtained for an increasing number of Rabi oscillations. A similar oscillating

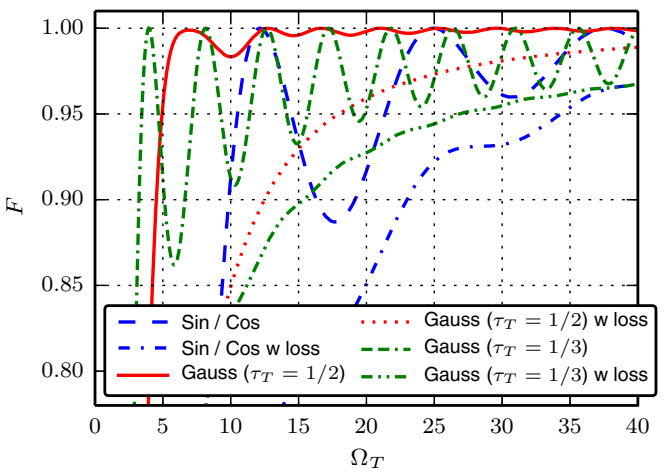

FIG. 4. (Color online) Fidelity vs Ω_T for STIRAP Gaussian and sin-cos protocols of Table I, the Gaussian ones with different values of τ_T. No loss ($\Gamma_2 = 0$) and with loss at $\Gamma_T = 4$.

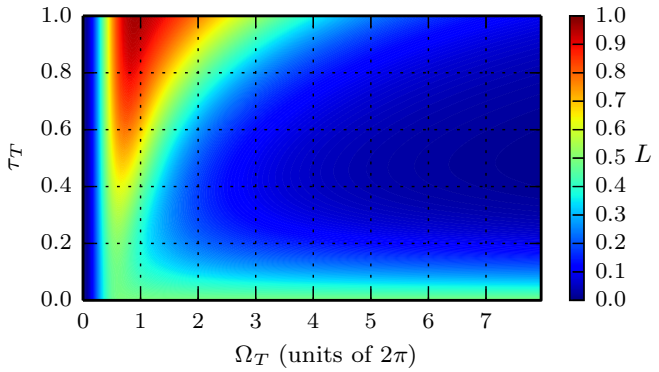

FIG. 5. (Color online) L STIRAP losses vs τ_T and Ω_T for Gaussian pulses with $\Gamma_T = 10$.

dependence of the fidelity on the protocol parameters was also found in Ref. [8] for a nonlinear Landau-Zener sweep.

The introduction of a loss rate for the $|2\rangle$ intermediate state decreases the fidelity because of losses all along the temporal evolution; see curves in Fig. 4 for the case of an open system.

B. Population loss

In presence of the Γ_2 loss rate the population loss to internal and external states during the system evolution is an important parameter of the transfer protocol. For a Γ_2 decay to external states that loss is given by

$$L = \Gamma_2 \int_{t_i}^{t_f} |\langle 2|\Psi(t)\rangle|^2 dt. \tag{29}$$

$(1 - F)$ represents a good approximation to this quantity, except for population left over in the $|1\rangle$ state. Figure 5 reports L results for Gaussian STIRAP transfers. Optimum transfer, i.e., L minimum, is produced for large Ω_T values and for an optimum τ_T. These losses are totally eliminated in sa-STIRAP protocols.

C. Robustness

In order to test the sensitivity of the STIRAP and sa-STIRAP protocols to a (simulated) variation in the control parameters, we varied the protocol parameters around the optimum value of the $\mathcal{F}$ fidelity.

In the case of $\Gamma_2 = 10/T$, i.e., a $|2\rangle$ decay rate much greater than T^{-1}, STIRAP and sa-STIRAP results for Gaussian pulses are compared in Fig. 6 as a function of τ_T and Ω_T. The STIRAP numerical results are in Fig. 6(a) and the bottom surface of (c). The $F > 0.999$ requirement is not satisfied in the explored range of delay and Rabi frequency values. The (a) and (b) plots evidence out that in the presence of the Γ_2 loss all the fidelity contours shrink in space and a high fidelity requires larger Rabi frequencies. Similar F tests for the sa-STIRAP protocol, assuming the application of the Ω_d pulse, are in Fig. 6(b) and the top surface of (c), while L losses are plotted in (d). In all these plots the detuning pulse remains locked at its value for $\tau_T = 1/2$, and that demonstrates that very high fidelities, and very small losses, are reached even if the detuning pulse is not perfectly matched at the value given by Eqs. (19) and (4). As a test of the sa-STIRAP robustness, from the area in Fig. 6(b) we derive that the the $F > 0.999$ condition is verified when

$$\Delta\tau/\tau < 0.35, \quad \Omega_T > 2. \tag{30}$$

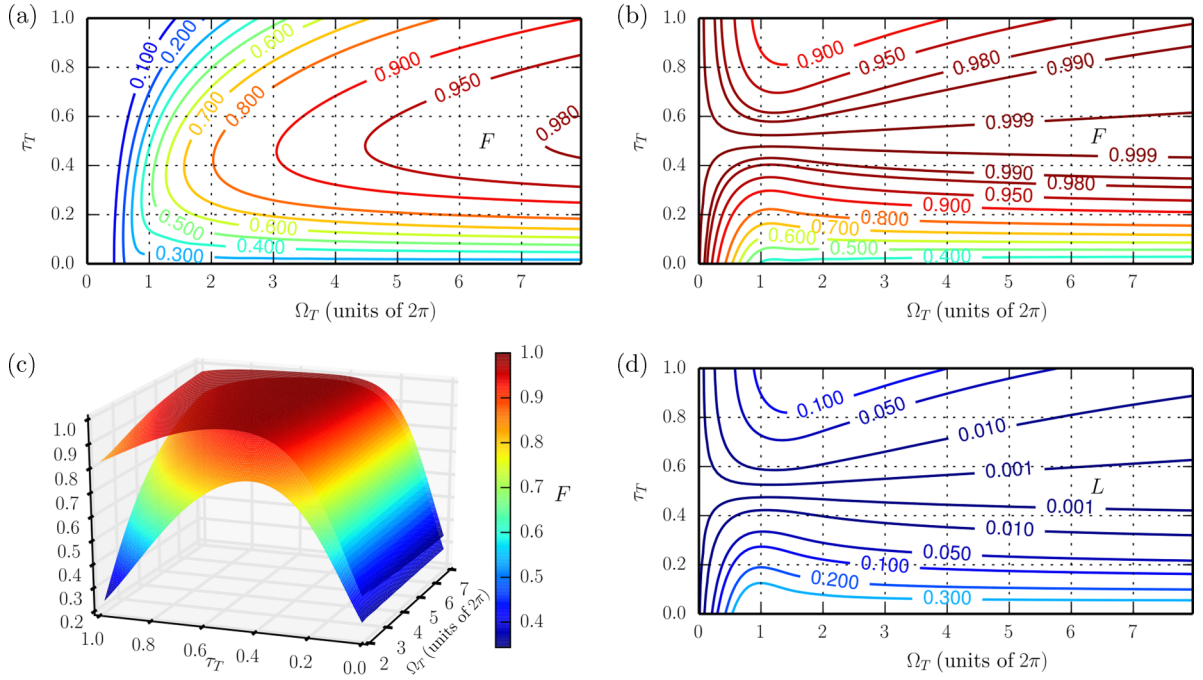

FIG. 6. (Color online) F and L vs τ_T and Ω_T for STIRAP and sa-STIRAP Gaussian pulses at $\Gamma_T = 10$. Fidelity F in (a) and (b) two-dimensional (2D) plots, and in 3D surfaces of (c). Losses L in 2D plot (d). In (a) and bottom surfaces of (c) for STIRAP protocols; in (b), top surface of (c) and (d) for sa-STIRAP protocols. For the sa-STIRAP's F deviates from one and L from zero because the detuning pulse is blocked at its value for $\tau_T = 1/2$.

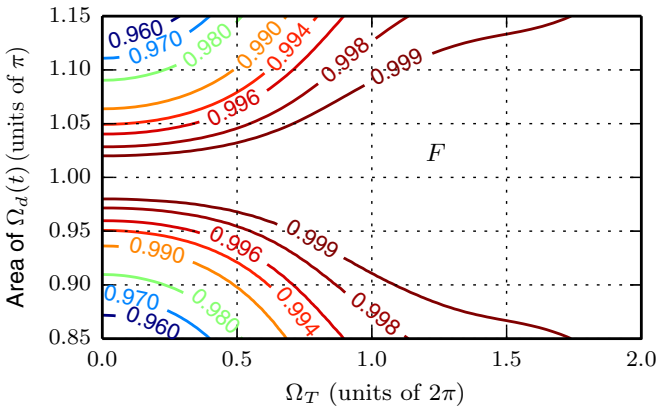

FIG. 7. (Color online) 2D plot of the sa-STIRAP fidelity vs Ω_T and the detuning pulse area around the π optimal value, for Gaussian pulses with $\tau_T = 0.5$ and $\Gamma_T = 1$.

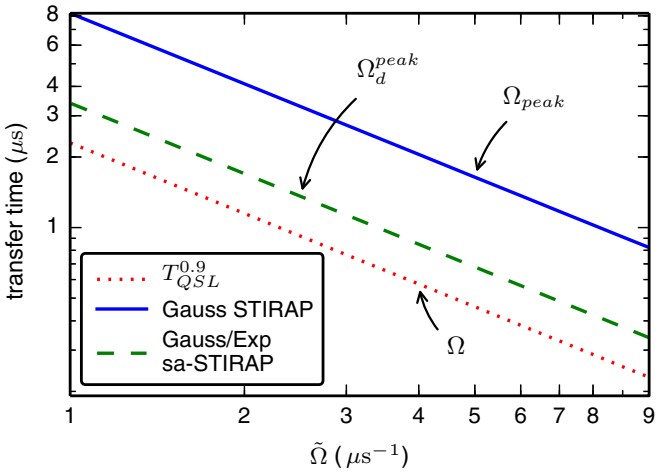

FIG. 8. (Color online) Three-level $T^{0.9}$ transfer time vs a characteristic $\tilde{\Omega}$ Rabi frequency. In the top vs $\tilde{\Omega} = \Omega_{\text{peak}}$ for the Gaussian STIRAP protocol with optimized T and τ parameters. In the center line vs $\tilde{\Omega} = \Omega_d$ peak value for the Gaussian or exponential sa-STIRAP protocols. In bottom line vs the $\tilde{\Omega} = \Omega$ Rabi frequency of a $|1\rangle$ and $|3\rangle$ direct coupling for the quantum speed limit, this limit reached also by the sa-sin-cos protocol with $\tilde{\Omega} = \Omega_d$. $\Gamma_2 = 0$ everywhere.

In Fig. 7 the fidelity is plotted varying both the detuning pulse area and the pump and Stokes maximum Rabi frequency. Those results show that the presence of the pump and Stokes pulses makes the π-area pulse more robust against a variation of its area. Finally testing under the same conditions the robustness of the detuning pulse phase, we found that the $F > 0.999$ condition is verified for a detuning phase different from π less than $\pi/40$ in the worst condition of $\Omega_T \approx 0.7$. At smaller (larger) Ω_T values the detuning pulse (the pump and Stokes pulses) dominate the system evolution and the stability conditions are more relaxed.

The plots of Fig. 4 indicate the limited robustness of the Gaussian and sin-cos STIRAP protocols produced by the oscillating behavior: the $F > 0.999$ condition requires a Ω_T control around 3%.

D. Protocol quantum speed

We investigate here the time required for the three-level quantum transfer. We define the three-level quantum transfer time $T^{0.9}$ as the time interval between the 99% occupation of the initial and the 90% occupation of the final $|2\rangle$ state. This definition does not match the standard one with an initial total occupation of the $|1\rangle$ state [25], in order to deal with the STIRAP protocols switched on at $t = -\infty$. Our results of $T^{0.9}$ vs the Ω_{peak} value for the Gaussian protocol are plotted in Fig. 8. For each data point both the T and τ_T values were optimized.

We compare those data to the quantum speed limit required for the three-level transfer. The previous analyses on the quantum speed limit in two-level systems [7,8,25] have demonstrated that the quantum speed limit is reached by a NMR-type π pulse, with constant Rabi frequency. Taking into account our initial and final conditions on the state occupation for a π pulse we obtain the following relation between the quantum speed limit time $T_{\text{QSL}}^{0.9}$ and the applied Rabi frequency Ω:

$$T_{\text{QSL}}^{0.9} = \frac{2.29}{\Omega}. \tag{31}$$

If Ω is nonconstant, the denominator of the above equation should be replaced by its time average. $T_{\text{QSL}}^{0.9}$ is plotted in Fig. 8 vs the Ω amplitude of an electromagnetic field producing the direct transfer between initial and final states given by Eq. (19). None STIRAP transfer is faster than the quantum speed limit. The difference between the quantum speed limit (QSL) and STIRAP transfer times greatly depends on the temporal superposition of the pump and Stokes pulses.

The temporal evolution of all sa-STIRAP protocols is determined by the $\Omega_d(t)$ detuning pulse. The associated transfer time is derived from Eq. (31) by inserting the time average value of Ω_d

$$T^{0.9} = \pi \frac{t_{0.9}^f - t_{0.99}^i}{\int_{t_{0.99}^i}^{t_{0.9}^f} \Omega_d(t) dt}, \tag{32}$$

where $t_{0.99}^i$ and $t_{0.9}^f$ are the initial and final times, respectively, where fidelity reach those values. Because of the area relation of Eq. (21) the Ω_d temporal average is very close to π, and therefore the transfer time depends on the temporal evolutions of Ω_d reported in column 3 of Table I. Both T and τ parameters appear in those evolutions, and for each protocol the transfer time has a specific dependence on the parameters. Notice that for the sa-sin-cos protocol, where a constant $\Omega_d = \pi/T$ pulse is applied (see line 5 of Table I), the speed limit of Eq. (31) is reached. In the case of the sa-sin^4 protocol the transfer time depends on τ_T reaching $T^{0.9} = 1.10(3) T_{\text{QSL}}^{0.9}$ at $\tau_T = 1/15$. For the Gaussian or exponential pulses $T^{0.9} = 1.48(3) T_{\text{QSL}}^{0.9}$, independently of τ_T. Finally for the sa-sin-cos(arctan) protocol, line 4 of Table I, not containing the τ parameter, $T^{0.9} = 2.73(5) T_{\text{QSL}}^{0.9}$.

V. CONCLUSIONS

The present work determines the corrections to the STIRAP pulses required to produce a superadiabatic transfer with fidelity equal to 1 in a three-level system. Each STIRAP

protocol has a different superadiabatic correction. The superadiabatic Hamiltonian requires the application of the detuning pulse as a direct coupling between the initial and final states. For the Λ level scheme a magnetic field, and for the ladder configuration a two-photon transition with laser fields created as radio frequency sidebands from the pump and Stokes laser beams, will produce that coupling. That direct interaction should be applied in a π-area, or near π-area, pulse configuration, and the application of the detuning pulse alone could produce the desired transfer. However, we demonstrate that the combination of STIRAP and detuning pulse has a robustness much larger than each separate transfer. The sa-STIRAP transfer occurs within a temporal window imposed by the applied detuning pulse. Transfer times close to a three-level quantum speed limit may be reached.

Even if the technical effort, and the energy requirement, required to realize a sa-STIRAP protocol may be considerable, its implementation is very useful in quantum driving realizations with heavy requirements of efficiency and stability. The application of additional electromagnetic fields is required, for instance, also in the robust composite stimulated Raman adiabatic passage proposed in Ref. [15]. We conclude that any gain in fidelity and in stability requires additional resources in experimental tools and laser power irradiating the sample.

ACKNOWLEDGMENTS

This work was supported by the PRIN-2009 Project Quantum Gases beyond Equilibrium of the MIUR-Italy and by the EU Marie Curie ITN COHERENCE. The authors thank R. Mannella and P. Pillet for useful discussions and suggestions, and D. Ciampini for a careful exam of the manuscript.

APPENDIX: DETUNING PULSE WITH PHASE CONTROL OF PUMP AND STOKES PULSES

This Appendix examines the sa-STIRAP Hamiltonian by introducing temporal dependencies for the phases of the pump and Stokes Rabi frequencies:

$$\Omega_p(t) = e^{i\phi_p(t)}|\Omega_p(t)|, \quad \Omega_s(t) = e^{i\phi_s(t)}|\Omega_s(t)|. \tag{A1}$$

Assuming $\Delta_p(t) = 0$, as in Eq. (17), in order to have $H^1(t)_{12}$ and $H^1(t)_{23}$ identically zero, the superadiabatic Hamiltonian of Eq. (12) for the ladder system becomes

$$H(t) = \frac{\hbar}{2}\begin{pmatrix} 0 & \Omega_p^*(t) & i\Omega_d^*(t) \\ \Omega_p(t) & 0 & \Omega_s^*(t) \\ -i\Omega_d(t) & \Omega_s(t) & 0 \end{pmatrix}, \tag{A2}$$

and for the Λ one

$$H(t) = \frac{\hbar}{2}\begin{pmatrix} 0 & \Omega_p^*(t) & i\Omega_d^*(t) \\ \Omega_p(t) & 0 & \Omega_s(t) \\ -i\Omega_d(t) & \Omega_s^*(t) & 0 \end{pmatrix}. \tag{A3}$$

In a definition of the detuning pulse more general than in Eqs. (19) and (4), here

$$\begin{aligned} \frac{\Omega_d(t)}{2} &= \frac{\dot\Omega_p(t)\Omega_s(t) - \Omega_p(t)\dot\Omega_s(t)}{|\Omega_p(t)|^2 + |\Omega_s(t)|^2} \quad \text{for ladder,} \\ \frac{\Omega_d(t)}{2} &= \frac{\dot\Omega_p(t)\Omega_s^*(t) - \Omega_p(t)\dot\Omega_s^*(t)}{|\Omega_p(t)|^2 + |\Omega_s(t)|^2} \quad \text{for } \Lambda. \end{aligned} \tag{A4}$$

For the ladder system the detuning may be written as

$$\begin{aligned} \frac{\Omega_d(t)}{2} = e^{i(\phi_p+\phi_s)}&[|\Omega_p(t)|^2 + |\Omega_s(t)|^2]^{-1} \\ &\times [|\dot\Omega_p(t)||\Omega_s(t)| - |\Omega_p(t)||\dot\Omega_s(t)| \\ &+ i(\dot\phi_s - \dot\phi_p)|\Omega_p(t)||\Omega_s(t)|]. \end{aligned} \tag{A5}$$

In order to reduce the detuning pulse we obtain an additional condition on the pump and Stokes phases, $\dot\phi_s = \pm\dot\phi_p$ in the ladder/Λ schemes respectively, or $\dot\phi_s = \dot\phi_p = 0$. However also with that phase control the sa-STIRAP protocol Ω_d cannot be identically zero.

[1] R. Lim and M. V. Berry, J. Phys. A: Math. Gen. **24**, 3255 (1991).
[2] M. Berry, J. Phys. A: Math. Theor. **42**, 365303 (2009).
[3] M. Demirplak and S. A. Rice, J. Phys. Chem. A **107**, 9937 (2003).
[4] M. Demirplak and S. A. Rice, J. Phys. Chem. B **109**, 6838 (2005).
[5] M. Demirplak and S. A. Rice, J. Chem. Phys. **129**, 154111 (2008).
[6] E. Torrontegui, S. Ibáñez, S. Martínez-Garaot, M. Modugno, A. del Campo, D. Guéry-Odelin, A. Ruschhaupt, X. Chen, and J. G. Muga, in *Advances in Atomic, Molecular, and Optical Physics*, edited by E. Arimondo, P. R. Berman, and C.C. Lin (Academic, Oxford, 2013), Vol. 62, pp. 117–169.
[7] M. G. Bason, M. Viteau, N. Malossi, P. Huillery, E. Arimondo, D. Ciampini, R. Fazio, V. Giovannetti, R. Mannella, and O. Morsch, Nat. Phys. **8**, 147 (2011).
[8] N. Malossi, M. G. Bason, M. Viteau, E. Arimondo, R. Mannella, O. Morsch, and D. Ciampini, Phys. Rev. A **87**, 012116 (2013).
[9] N. Malossi, M. G. Bason, M. Viteau, E. Arimondo, D. Ciampini, R. Mannella, and O. Morsch, J. Phys.: Conf. Ser. **442**, 012062 (2013).
[10] J. Zhang, J. H. Shim, I. Niemeyer, T. Taniguchi, T. Teraji, H. Abe, S. Onoda, T. Yamamoto, T. Ohshima, J. Isoya, and D. Suter, Phys. Rev. Lett. **110**, 240501 (2013).
[11] K. Bergmann, H. Theuer, and B. Shore, Rev. Mod. Phys. **70**, 1003 (1998).
[12] P. Král, I. Thanopulos, and M. Shapiro, Rev. Mod. Phys. **79**, 53 (2007).
[13] X. Chen, I. Lizuain, A. Ruschhaupt, D. Guéry-Odelin, and J. G. Muga, Phys. Rev. Lett. **105**, 123003 (2010).
[14] R. Unanyan, L. Yatsenko, K. Bergmann, and B. Shore, Opt. Commun. **139**, 48 (1997).
[15] B. T. Torosov and N. V. Vitanov, Phys. Rev. A **87**, 043418 (2013).
[16] X. Chen and J. G. Muga, Phys. Rev. A **86**, 033405 (2012).

[17] B. Shore, *The Theory of Coherent Atomic Excitation* (John Wiley & Sons, Inc., New York, 1990).
[18] T. A. Laine and S. Stenholm, Phys. Rev. A **53**, 2501 (1996).
[19] M. Fewell, B. Shore, and K. Bergmann, Austr. J. Phys. **50**, 281 (1997).
[20] M. Elk, Phys. Rev. A **52**, 4017 (1995).
[21] M. Fleischhauer, R. Unanyan, B. W. Shore, and K. Bergmann, Phys. Rev. A **59**, 3751 (1999).
[22] C. E. Carroll and F. T. Hioe, Phys. Rev. A **42**, 1522 (1990).
[23] M. Fleischhauer and A. S. Manka, Phys. Rev. A **54**, 794 (1996).
[24] E. Brion, L. H. Pedersen, and K. Mølmer, J. Phys. A: Math. Theor. **40**, 1033 (2007).
[25] V. Giovannetti, S. Lloyd, and L. Maccone, Phys. Rev. A **67**, 052109 (2003).